


Dynamic finite element analysis of rotor-shaft fastening into a heavy precise lathe

Stanislau Dounar¹, Andrzej Jakubowski²✉

¹  <https://orcid.org/0000-0002-6201-8340>

²  <https://orcid.org/0000-0002-0331-3147>

¹ Belarusian National Technical University, Mechanical Engineering Faculty
65 Nezalezhnasci St., 220127 Minsk, Belarus

² Maritime University of Szczecin, Faculty of Marine Engineering
1-2 Waly Chrobrego St., 70-500 Szczecin, Poland
e-mail: a.jakubowski@am.szczecin.pl

✉ corresponding author

Keywords: finite element analysis (FEA), lathe, rotor, renovation, rigidity, reinforcement

JEL Classification: C630, L600, L610

Abstract

The results of finite element analysis of large machined rotor fastened into heavy precise lathe are reported. Many design changes are simulated to improve the dynamic rigidity of the machining. Three radial eigenmodes detrimental to the accuracy were revealed: rotor-stock bending at 17.7 Hz (“half-wave”), rotor-lathe bending at 36.1 Hz (“full-wave”), and “support rocking” at 68.1 Hz. The frequency response functions and dynamic rigidities were evaluated. Three compliance issues were revealed: angular flexibility of the spindle console, low stiffness of the lathe bed (with boots), and an excessively slender tailstock. It is proposed to transform the spindle chuck into a table with additional hydrostatic backing, fill the bed cavities with concrete, and redesign the tailstock as a counter-spindle unit. This will decrease the amplitude of the main rotor resonance by 6.3 times and upshift the frequency near two-fold from 17.7 to 35 Hz. The renovated lathe should be able to machine a rotor without a lunette system or overriding the main resonant frequency.

Introduction and aim of the work

Heavy precise lathes (HPLs) provide a unique possibility to perform the horizontal machining of large rotor-shafts for shipbuilding and energy industries. Such rotor-shafts are mostly needed for turbine machines and generators. Single HPLs provide full cutting due to the rough turning of forged rotor-shaft blanks to finishing with a tolerance near ± 0.01 mm, so they should be simultaneously robust and precise.

Huge lathes require accuracy and static rigidity (mainly for finishing), as well as dynamic rigidity (for rough cutting firstly). Few investigations have investigated the rigidity of large lathes (Dornfeld

& Lee, 2008; Choi, Ha & An, 2014). It is fruitful to perform computer simulations by finite element analysis (FEA) (Zienkiewicz & Taylor, 2000), which is effective at forecasting the rigidity of very different machine tools (López de Lacalle & Lamikiz, 2008; Anand & Roy, 2018), including heavy ones (Vasilevich et al., 2015; Vasilevich, Dounar & Karabaniuk, 2016).

Work has been conducted related to renovating a group of KZTS-branch large lathes. The project involved machine disassembly, replacing the main drive and feed drives, guideline revision, etc. The scope of such works makes it possible to reinforce the *load-bearing system* (LBS) of lathes, whose main

goal is to increase the static rigidity with dynamic rigidity. Quite different improvements may be proposed, which must be evaluated by FEA to recommend a design solution for LBS renovation.

Rotor-shafts demand precise turning twice during processing. The first stage of precise cutting ends up the bare rotor-shaft machining (mark it – *RotBare1*). The second stage takes place after rotor-shaft assembly with massive and chunky bush-like parts (*RotAssem2*). It may be turbine wheels, winding cages, etc. Such parts significantly affect the statics and dynamics of the lathe–rotor system.

There are two techniques to base (precisely fasten) the rotor-shaft while machining. The first consists of oppositely holding the rotor-shaft ends by the headstock and tailstock (*BasEnd1*). The second is related to several lunettes bearing rotor-shaft from its bottom (*BasLun2*). In this case, the headstock is needed only for torque transmission and provides a flexible coupling. Both techniques are used in practice as concurrent ways of basing.

During the renovation, the plan involved specializing separate HPLs from the group according to the processing stages (*RotBare1* or *RotAssem2*) and fastening technique (*BasEnd1* and *BasLun2*). At the same time, the possibility to rearrange supports by cutter units as high-speed milling heads was targeted. Switching from traditional turning cutters to high-speed mills is a modern trend. The milling head at the lathe support reduces cutting time and improves the surface quality, though this demands a higher dynamic rigidity of the machine tool.

Thus, several FEA investigations were accomplished in parallel. The paper in ref. (Dounar, 2017) optimized a lathe's static rigidity for a rotor end fastening (*BasEnd1*) and primary machining

(*RotBare1*). The dynamic rigidity of the lunette-bearing rotor-shaft (*BasLun2*) is considered (*RotBare1*) in another (Vasilevich & Dounar, 2017). The papers (Dounar et al., 2018a; Dounar, Iakimovitch & Jakubowski, 2020) revealed the statics and dynamics of an assembled rotor-shaft (*RotAssem2*) in the case of mixed basing by ends and upon lunettes (*BasEnd1* + *BasLun2*). That pair of works, in conjunction with the investigation of a lathe's support rigidity (Dounar et al., 2018b), analyzed the possibility to raise the centerline, which should allow the machining of rotor-shafts with larger diameters (up to $\phi 3000$ mm).

This work aims to investigate lathe dynamics during the machining of a rotor-shaft (*RotBare1*) held by its ends (*BasEnd1*) and to reveal design solutions for increasing the dynamic rigidity of lathe–rotor systems. The work continues the investigation in (Dounar, 2017) from the static field to the dynamic one.

Lathe geometry

Figure 1 shows a machined rotor-shaft R (below – rotor) fastened horizontally between the *headstock* (HS) and *tailstock* (TS). From 1 to 3, the *support* (S) may be placed upon guideways on *bed* (B). Supports are depicted at three reference positions *a1*, *b2*, and *c3*. The positions are related to three systems of reference rotor belts (*rrb*) on the rotor surface. Belts (precise grooves) are necessary for rotor measuring and alignment. The human figure (Figure 1) emphasizes the lathe dimensions. Table 1 presents data concerning the dimensions and masses of the lathe-rotor system.

The lathe axes are oriented according to *computerized numerical control* (CNC) standards: X – radial, Y – vertical, and Z – axial (along spindle 1

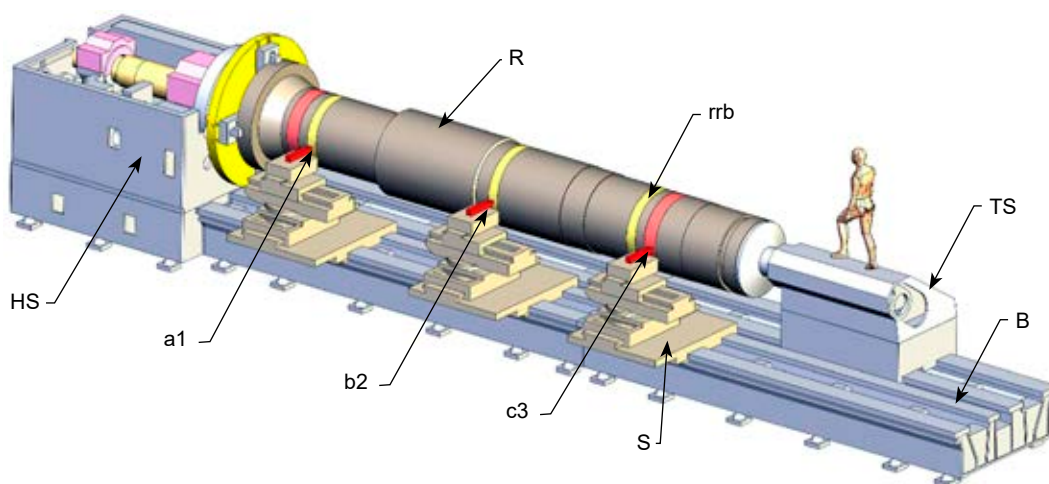


Figure 1. Geometrical model of the HPL

Table 1. Lathe-rotor assembly data for FEA simulations

No. Object	Parameter	Value
1 Lathe itself	length	15.94 m
2	height	2.81 m (2.96 m from chuck top point to ground)
3	width	2.52 m
4	centerline	1060 mm above guidelines (1914 mm above ground)
5	weight	89.2 ton (drives excluding)
6 Rotor machined	length	8345 mm
7	diameter	$\phi 1204$ mm
8	weight	31.7 ton (36% of lathe mass)

and rotor 3 common axis). The radial direction X is preferred in this work for machining precision. Any radial displacement of the rotor or support transforms directly with double scale relative to the diametrical inaccuracy of the rotor.

Figure 2 shows the main (lowest) eigenmode $Mh1$, found by FEA at a frequency of 17.78 Hz. It may be excited by cutting forces between the tool and rotor. There is a flexible line, going from spindle 1 with chuck 2 through rotor 3 to tailstock 5. The rotor, headstock, and tailstock are all involved in bending in horizontal plane XZ. The oscillation pattern is “half-wave” (half of a sinusoidal period) with an antinode at the middle of the rotor length (near $b2$ reference position and tool-holder 4). The tool-holder (with cutter or mill) reciprocates radially into the guideways of support 6. The support is not involved in the resonance pattern.

Tailstock 5 locally deforms bed 7. Lathe boots 8 significantly distorts under stocks. The bed system visually appears excessively compliant. So, the *first*

renovation proposition may be stated – to increase bed rigidity and enhance its binding to the basement (not shown, taken motionless).

The headstock (Figure 3) holds chuck 1 and spindle 5 by the front rest 3 and rear rest 6 with rolling bearings between. Chuck 1 and spindle 5 form a single part and are separated only for repair. The chuck serves as the table for rotor alignment and fastening. The assembly of the spindle and chuck will be called the *T-spindle*, which rotates most of the machining time at a low frequency ($\leq 100 \text{ min}^{-1}$) and high torque; therefore, the *T-spindle* is driven originally, by the toothed wheel pair 3, directly to the chuck.

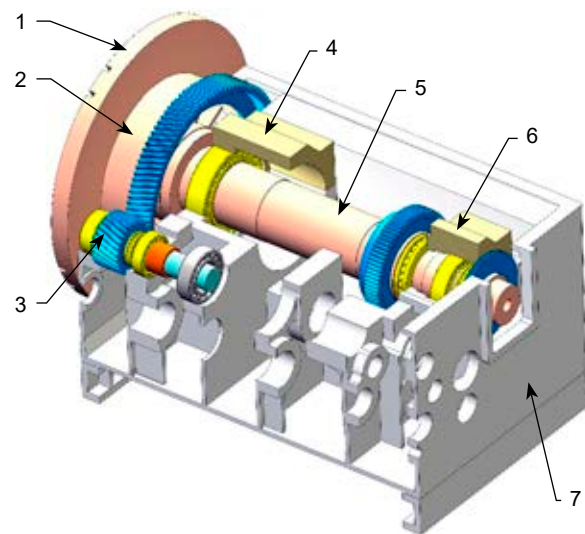


Figure 3. The headstock of HPL: 1 – chuck (rotary table in effect), 2 – chuck areas convenient for backing, 3 – driving toothed wheels, 4 – front spindle rest, 5 – spindle, 6 – rear spindle rest, 7 – casing

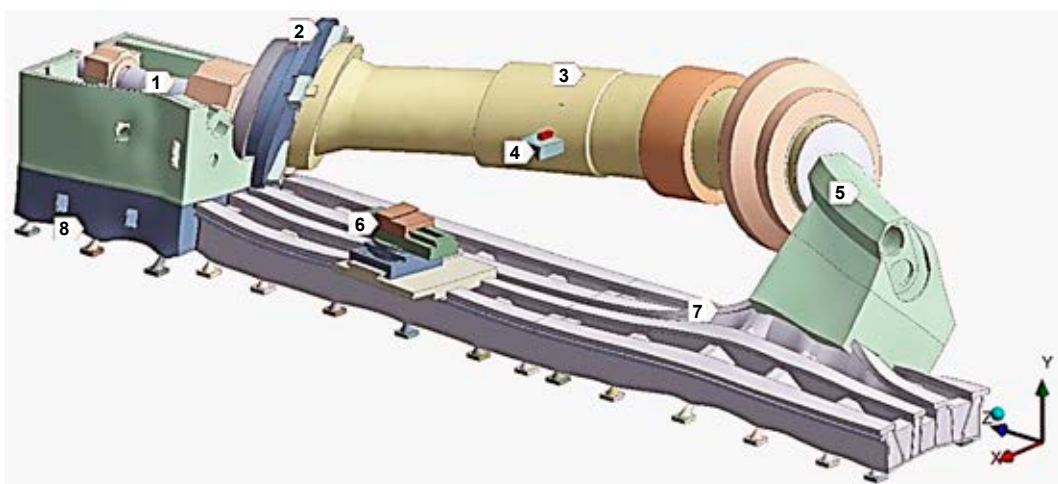


Figure 2. FEA-model of the HPL during resonance by horizontal bending eigenmode $Mh1$ (17.78 Hz): 1 – spindle into headstock bearing rests, 2 – chuck (table), 3 – machined rotor (rotor-shaft), 4 – tool into tool-holder, 5 – tailstock, 6 – support as slider pile, 7 – bed, 8 – boot

The span between chuck 1 and front rest 4 is called the *spindle console*. Figure 2 shows the loss of chuck orthogonality to the initial lathe axis (markers 1 and 2), which is due to the low angular rigidity of the *spindle console*. Usual issues are spindle bending and front rest bearing angular pliability.

Second renovation proposition – to abut the chuck directly onto casing 7 through cylindrical and butt surfaces in region 2 (Figure 3). Hydrostatic radial and thrust bearings (Rowe, 2012; Fedorynenko, Sapon & Boyko, 2016) are near the single choice for that. This modification will be called the below *peripheral chuck backing* (PCB), and it should convert the chuck into a steady rotary table. The flexibility of the *spindle console* may be eliminated.

Simulated lathe reinforcement variants

The simulation's main task is to reveal dynamically rigid rotor fastening variants. Next, the variants must be designed (*design measures*) to reinforce the lathe parts that have been simulated:

- V1 – initial lathe state (Figures 1, 2, 3);
- V2 – bed rigid fixation upon basement (boots flexibility excluded);
- V2a – variant V2 plus polymer concrete filling of bed cavities (Vasilevich, Dounar & Karabaniuk, 2016; Simon, Grama & Ganea, 2012) (bed becomes a rigid body);
- V3 – excessive rigidity of spindle bearings into the front and rear rests (only spindle pliability – mainly *spindle console* bending – takes part in rotor deformations; excessive rigidity may be achieved by placing hydrostatic bearings instead of rolling ones);
- V4 – PCB;
- V5 – tailstock bottom connection across the bed with all guideways (achieved using FEA; estimates massive counter-spindle unit mounting instead of a relative slender tailstock).

FEA model, techniques, and parameters

The main design material for the lathe is cast iron with an elasticity modulus $E_{ci} = 130$ GPa (Table 2). The bed and stock casings are made from it. The rotor, spindle, and chuck (table) are simulated as steel parts with an elasticity modulus $E_{st} = 200$ GPa. The front and rear bearings are modeled as sleeves made of a special modeling material, whose parameters are tuned by the special test (Vasilevich et al., 2015; Vasilevich & Dounar, 2017). Boots under the

bed are shaped like cones made from another modeling material. The single boot rigidity was equal to 3700 N/ μm in the vertical direction and 1050 N/ μm in any horizontal one. This matches preliminary *in situ* lathe tests. The rotation of the rotor, spindle, and chuck were not modeled.

Table 2. Material's mechanical properties

No.	Modeling material	Young's modulus E (GPa)	Poisson's ratio μ (–)	Specific density ρ (kg/m ³)
1	Cast iron	130	7200	0.28
2	Steel	200	7850	0.3
3	Polymer concrete	25–35	2200	0.18
4	Material for spindle bearings	4	3800	0.3
5	Boot material	30	2300	0.2

The FEA model consists of 119 separate meshes according to the number of solids in the geometry models. Numerous contact pairs were created between meshes. The status *bonded* (strong sticking between adjacent surfaces) was stated for the majority of contact pairs. The status *no separation* (sliding without friction and contact opening) was designated for a few contact pairs in the simulated guideways. Frictional contacts were not used because they are not allowable for classic modal and harmonic analyses, provided below.

The model is fully linear. Geometrical nonlinearities are neglected since significant displacements during loading are not expected. Plastic nonlinearity is not taken into account due to the low level of stress, which is common for heavy machine tools, so it was checked by preliminary HPL tests.

HPL modal analysis

Modal FEA was provided for a frequency interval up to 100 Hz, which is sufficient to reveal all whole-lathe eigenmodes for the heavy machine. Eight such eigenmodes were found (Table 3), all with frequencies below 70 Hz. Some modes are not related to the radial direction (e.g., torsional mode m_{tors1} and axial one m_{ax1}) and are not discussed in this work.

Three eigenmodes demand attention first: $Mh1$ (Figure 2), $Mh2$ (Figure 4a), and $Msup1$ (Figure 4b). Modes $Mh1$ and $Mh2$ are related to rotor resonances with flexible line bending in the horizontal plane XZ. Resonance by $Mh1$ consists of a “half-wave” oscillation of the rotor and stocks. Resonance $Mh2$ is excited according to the “full-wave” pattern. The flexible line A-B-C-D is near full period sinusoidal

Table 3. Lathe eigenmodes in the frequency interval 0–70 Hz

No.	Frequency (Hz)	Sign	Rotor or support deformation pattern
1	17.78	<i>Mh1</i>	Halve-wave horizontal bending
2	26.37	<i>mv1</i>	Halve-wave vertical bending
3	31.28	<i>m_tors1</i>	Torsional oscillation about rotor axis
4	36.11	<i>Mh2</i>	Full-wave horizontal bending
5	38.52	<i>m_ax1</i>	Axial oscillations along the rotor axis
6	54.47	<i>mv2</i>	Full-wave vertical bending
7	58.94	<i>m_hv1</i>	Mixed vertical and horizontal full-wave rotor weaving
8	68.16	<i>Msup1</i>	Support oscillation in the radial direction

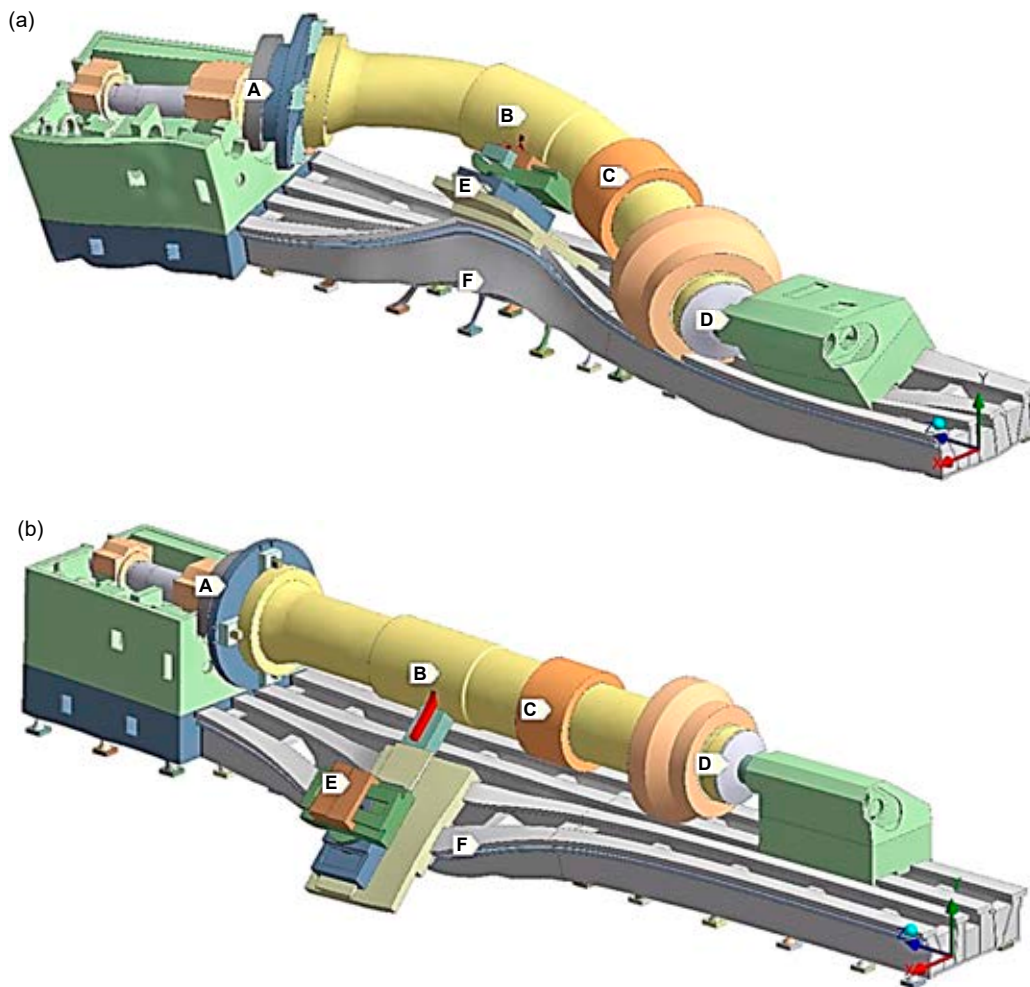
with 3 nodes – deep in the headstock and in the tailstock, as well as in the middle of the rotor (*b2*). The antinodes coincide with reference positions *a1* and *c3* at the rotor ends.

The vertical rotor bending resonant modes are disclosed for plane YZ – *mv1* and *mv2*. They are similar to horizontal eigenmodes *Mh1* and *Mh2*,

respectively. The vertical resonances are not deliberated in this work. Vertical oscillation is tangential to the rotor surface near the tool cutting zone, so inaccuracies created are lower in order compared with radial movements (by eigenmodes *Mh1* and *Mh2*).

The rotor resonance involves the headstock and tailstock. The *T-spindle*, rotor, and tailstock quill established a unified flexible axis (A-B-C-D in Figure 4a). This points out the excess pliability of both stocks and the bed below.

The main support resonance according to mode *Msup1* is revealed (Figure 4b). Support E oscillates in plane XY along with both vertical and horizontal directions. The compliance of the underlying bed F is the issue. Eigenmode *Msup1* is very detrimental to machining precision, but there is a near octave clearance between the support and rotor neighboring resonances. The rotor flexible line (A-B-C-D at Figure 4b) stayed straight during support excitation, so there is no essential crossing between the rotor and support resonant movements. It is the dignity of lathe investigated.


Figure 4. Excited eigenmodes *Mh2* (a) 36.11 Hz and *Msup1* (b) 68.16 Hz

Harmonic analysis of the lathe

Two forces, equal by value but opposite in direction, were applied to the cutting tool in the support and the adverse area on the rotor surface. They were radially aligned (X) harmonic forces: $F_t = A \sin(2\pi f_h t)$ for tool and $F_r = -A \sin(2\pi f_s t)$ for the rotor. Here, $A = 1000$ N – amplitude of forced oscillation; f_s – simulation test frequency; t – time.

Paired forces oscillate in the counter-phase and balance each other in the lathe span. Tests were conducted in the frequency interval from 0 to 100 Hz, which is sufficient to reveal the excitement of all “whole-lathe” resonances. The damping ratio $\zeta = 2\%$ was assumed to be uniformly distributed throughout all machine parts. The radial displacements on the tool and reference rotor belts were the output data for corresponding *frequency response functions* (FRF). Support harmonic excitation was investigated in a separate work (Lopez de Lacalle & Lamikiz, 2008; Dounar et al., 2018b). Hereinafter, only a rotor with stocks is preferably discussed.

The bed was simulated as filled with polymer concrete (reinforcement measure $v2a$), which

substantially weakened bed distortions. Figure 5 shows radial FRF's for three reference belts 1a, 2b, and 3c. Resonance peaks $Mh1$ and $Mh2$ are observed. The lowest resonance $Mh1$ is the strongest one. Intervals near peaks will be noted as pre-resonant ($Int1$), inter-resonant ($Int2$), and post-resonant ($Int3$). The excitement of $Mh1$ is essential for the precision of the rotor middle part (curve 2b). The amplitudes of $Mh1$ and $Mh2$ resonances are comparable to each other near rotor ends (curve 1a for headstock end and 3c for tailstock one).

The reference belt amplitudes are inversely proportional to dynamic rigidities $J_{a1,b2,c3}$ in corresponding places, and they are strictly dependent on the current frequency. Table 4 shows the dynamic rigidities only for resonant frequencies and for ones in the middle of intervals $Int1$, $Int2$, and $Int3$. The middle reference position 2b is mentioned twice – for reinforcement variants $v2a$ and $v4$.

Table 4 shows the allowable machining into “ $Int2$ ” and “ $Int3$ ” intervals. The dynamic rigidities at all reference positions are higher compared with the near-static “ $Int1$ ” interval. This is connected with the effect of post-resonance damping.

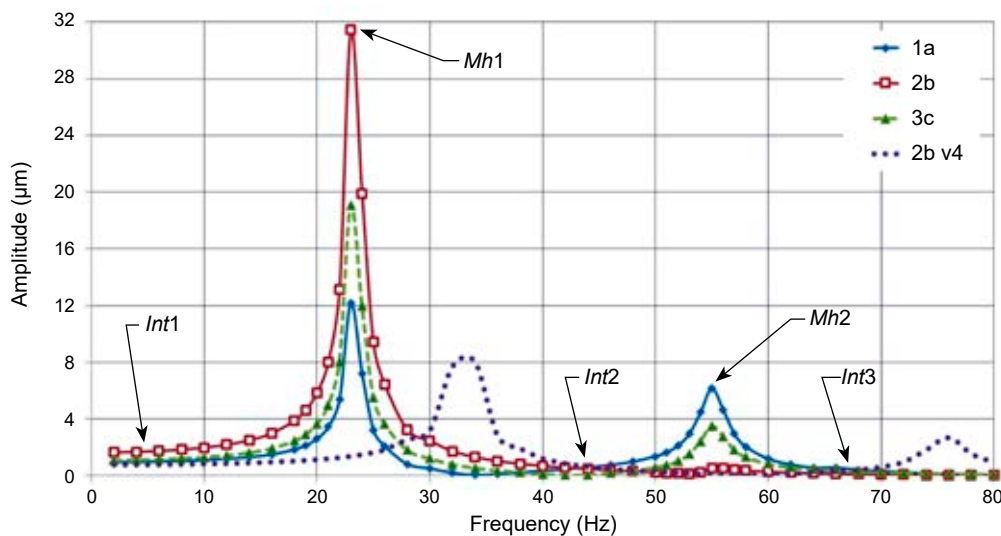


Figure 5. Lathe FRFs at reference positions 1a, 2b, and 3c in the case of bed rigid fixation ($v2a$). The line “2b v4” is related to support position 2b in the case of additional peripheral chuck backing ($v4$)

Table 4. Dynamic rigidity at reference rotor belts for $V2a$ and $V4$ reinforcement variants

Frequencies f and rigidities J	$Int1$ (near static)	$Mh1$	$Int2$ (inter-resonance)	$Mh2$	$Int3$ (post-resonance)
f_s (Hz) ($V2a$)	10	23	40	55	70
J_{a1} (N/ μ m)	900	9%	312%	18%	335%
J_{b2} (N/ μ m)	502	6%	283%	376%	1830%
J_{c3} (N/ μ m)	754	7%	936%	37%	532%
J_{b2}^{V4} (N/ μ m)	1214	10%	870%	31%	400%
f_s (Hz) ($V4$)	10	34	55	76	100

Rigidity is specified in $N/\mu m$ for column “*Int1*” and in percent to this column for columns to the right of “*Int1*”. For example, the rigidity is equal to $502 N/\mu m$ for the middle of the rotor (string J_{b2}) in the near-static conditions (column “*Int1*”; low frequency of excitation – 10 Hz). This is quite a high magnitude to ensure rotor machining accuracy. Then, the dynamic rigidity falls to 6% at the main resonance (column “*Mh1*”; frequency $f_s^{Mh1} = 23$ Hz, rigidity $J_{b2}^{Mh1} = 32 N/\mu m$ only). It is a near-threshold quantity [$J_{tres} = 20 N/\mu m$ (Dounar, 2017)]. Self-oscillations may be induced from the cutting zone with the loss of tool-rotor interface stability (Jafarzadeh & Movahhedy, 2017; Muhammad et al., 2017).

PCB (measure *V4*; string J_{b2}^{V4} in Table 4) increased the pre-resonant rotor rigidity 2.4 times – to $1214 N/\mu m$ (column “*Int1*”). The rigidity decreased again at *Mh1* resonance frequency, but 10% remained (column “*Mh1*”). This means that the rigidity $J_{b2,PCB}^{Mh1} = 124 N/\mu m$ is much higher than the $20 N/\mu m$ threshold.

Machining at the resonance frequency often is named “resonance overriding”. Overriding *Mh1* is dangerous to variant *V2* (Table 4) and vice versa is appropriate under the PCB condition (*V4*).

Figure 6 depicts the rotor/support dynamics for the basic variant (*v1r*, *v1s* curves) and bottom fixation (*v2r*, *v2s* curves) of the bed. The bed cavities are all empty. The bed pliability shifts the FRF’s curves in Fig. 6 to lower frequencies compared with Figure 5. Rigid bed bottom fixation only affects the support oscillation (eigenmode *Msup1*). The transition from design variant *V1* to *V2* increases the *Msup1* peak frequency from 52.5 to 90 Hz and at the same time dampens the peak amplitude by half from 46.4 to

$24.7 \mu m$. The rotor resonance *Mh2* “full-wave” is faintly influenced by bed bottom fixation. The main resonance *Mh1* “half-wave” is indifferent to this design measure.

Bed boot rigidity is satisfactory for rotor dynamics, but not for those of the support. The bed itself locally deforms under the support (Figure 4a and 4b – marker F). Thus, strengthening the boot system can be supplemented by pouring polymer concrete into the bed cavities. Both measures make the bed steady.

Figure 7 presents the influence of the reinforcement measures *V3*, *V4* (headstock), and *V5* (tailstock) on the rotor FRF. The FRFs amplitude is taken on the middle (position *b2*) and is inversely proportional to dynamic rigidity. Amplitudes, calculated just at rotor resonance frequencies, are collected in Table 5.

Table 5. Resonance peaks data for different lathe reinforcement variants

Reinforcement options		<i>V1</i>	<i>V3</i>	<i>V3+4</i>	<i>V3+4+5</i>
Statics	Amplitude, μm	2.14	1.42	0.6	0.51
	Excitation frequency, Hz	17.5	20	22.5	35
<i>Mh1</i>	Amplitude, μm	34.73	26.39	3.96	5.46
	Excitation frequency, Hz	35	50	60	77.5
<i>Mh2</i>	Amplitude, μm	3.59	4.92	4.21	3.37

Increasing the spindle bearing rigidity is not a sufficient measure. Curve *V3* in Figure 7 demonstrates only a small *Mh1* frequency upshift (14.2%) with moderate amplitude lowering (by 1.31 times). This is caused by the remaining spindle console flexibility.

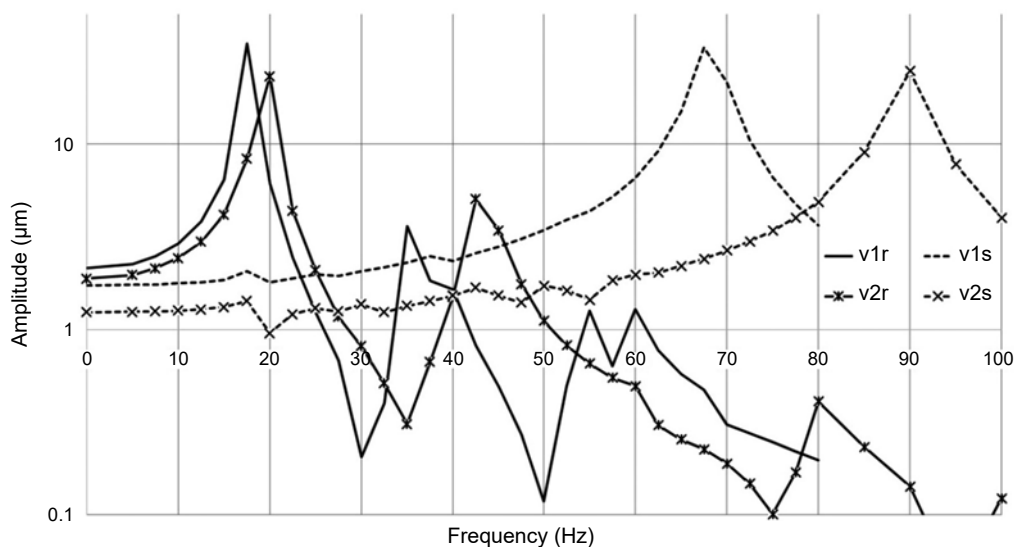


Figure 6. FRFs of the rotor (*v1r*, *v2r*) and support (*v1s*, *v2s*) for reinforcement variants: *V1* – basic, *V2* – rigidly fixed bed bottom

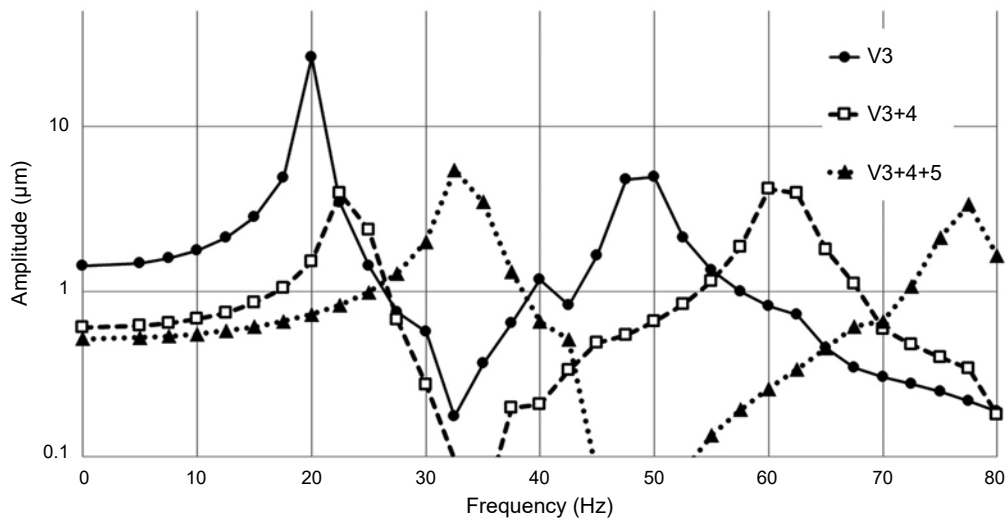


Figure 7. Rotor radial FRF curves for reinforcement according to design variants: *V3* – rigid spindle bearings; *V3+4* – combination of variants *V3* and *V4* (peripheral chuck backing – PCB); *V3+4+5* – enhancing *V3*, *V4* reinforcements by tailstock bottom strengthening by variant *V5*

FEA modeling shows the effectivity of peripheral chuck backing PCB (measure *V3*), which creates a rigid T-spindle by fixing the front *spindle console*. That console (range along spindle between front rest and chuck hub junction) is too angularly pliable. PCB increases the static radial rigidity 3.56 times (in the rotor middle). In dynamics, at resonance, *Mh1* amplitude decreased by 8.77 times. The rotor flexible line was prevented from propagating into the headstock. The last one became sufficiently monolithic.

Line “*V3+4+5*” shows why tailstock replacement by a massive counter-spindle stock is recommended. That measure (*V5*) increases the frequencies of all rotor eigenmodes and is fully compatible with measures *V3* and *V4*.

Conclusions

Three radial eigenmodes detrimental to the precision and stability of cutting are revealed: horizontal rotor-stocks bending mode *Mh1* “half-wave” at 17.78 Hz, akin “rotor-lathe” mode *Mh2* “full-wave” at 36.11 Hz, support rocking eigenmode *Msup1* at 68.16 Hz. A valuable lathe feature is an octave clearance between rotor and support resonance frequencies.

Bed reinforcement by polymer concrete pouring and direct bed-basement binding alleviates the support resonance peak *Msup1* and shifts its frequency to a higher frequency of 23 Hz. At the same time, the rotor resonances are rather unaffected to bed reinforcement. Eigenmode *Mh1* “Half-wave” frequency increased by only 6–7 Hz without peak damping.

For the *initial lathe state*, resonance *Mh1* is detrimental and cannot be “overridden” by machining frequency at a low dynamic rotor rigidity (28.7 N/µm). The excitement of eigenmode *Mh2* “full-wave” delivers diameter inaccuracies near rotor ends. Intermittent cutting by milling tools is appropriate *only* at post-resonant frequencies (≥ 70 Hz) or inside a narrow inter-resonant interval.

Peripheral chuck backing by the installation of hydrostatic radial and axial bearings is recommended because it results in abrupt resonance *Mh1* peak lowering by an order of magnitude. Machining by overriding the *Mh1* frequency became allowable.

The dynamic rigidity of the tailstock was insufficient. Thus, it is reasonable to transform the tailstock into a massive counter-spindle unit. Peripheral chuck backing for both spindle and counter-spindle permits turning and milling the rotor without lunette systems. The frequency of the main resonance *Mh1* upshifted from 17.7 to 35 Hz, and the rotor dynamic radial rigidity increased to 252.1 N/µm.

References

1. ANAND, A. & ROY, H. (2018) Static and Dynamic Analysis of Lathe Spindle using ANSYS. *International Journal of Applied Engineering Research* 13, 9, pp. 6994–7000.
2. CHOI, Y.H., HA, G.B. & AN, H.S. (2014) Stiffness Evaluation of a Heavy-Duty Multi-Tasking Lathe for Large Size Crankshaft Using Random Excitation Test. *Journal of the Korean Society for Precision Engineering* 31(7), pp. 627–634.
3. DORNFIELD, D. & LEE, D.-E. (2008) *Precision Manufacturing*. Springer.
4. DOUNAR, S.S. (2017) Virtual investigation of static deformations of the rotor-shaft into the extra heavy lathe. *Theoretical and Applied Mechanics* 32, pp. 72–78.

5. DOUNAR, S.S., IAKIMOVITCH, A.M., AUSIYEVICH, A.M. & JAKUBOWSKY, A. (2018a) FEA-analysis of shaft and supports deformations for huge precise lathe; statics and resonances. *New trends in productive engineering*, vol. 1, issue 1.
6. DOUNAR, S.S., IAKIMOVITCH, A.M., AZHAR, A.U. & KUCHYNSKAYA, N.A. (2018b) FEA analysis of heavy lathe support rigidity for statics and dynamics. *Mashinostroenie* 31. Minsk.
7. DOUNAR, S.S., IAKIMOVITCH, A.M. & JAKUBOWSKI, A. (2020) Finite Element Method analysis of the deformation of the shaft and supports of the large, precise lathe – Cutting force excitation. *Scientific Journals of the Maritime University of Szczecin, Zeszyty Naukowe Akademii Morskiej w Szczecinie* 62 (134), pp. 91–98.
8. FEDORYNENKO, D., SAPON, S. & BOYKO, S. (2016) Accuracy of Spindle Units with Hydrostatic Bearings. *Acta Mechanica et Automatica* 10(2), pp. 117–124.
9. JAFARZADEH, E. & MOVAHHEDI, M.R. (2017) Numerical simulation of the interaction of mode coupling and regenerative chatter in machining. *Journal of Manufacturing Processes* 27, pp. 252–260.
10. LÓPEZ DE LACALLE, L.N. & LAMIKIZ, A. (Eds) (2008) *Machine Tools for High Performance Machining*. Springer.
11. MUHAMMAD, B.B., WAN, M., FENG, J. & ZHANG, W.-H. (2017) Dynamic damping of machining vibration: a review. *International Journal of Advanced Manufacturing Technology* 89, pp. 2935–2952.
12. ROWE, W.B. (2012) *Hydrostatic, Aerostatic, and Hybrid Bearing Design*. Elsevier.
13. SIMON, M., GRAMA, A.L. & GANEA, M. (2012) *Study of improving static rigidity on machine tool structure using concrete component*. The 6th edition of the Interdisciplinarity in Engineering. International Conference “Petru Maior” University of Țirgu Mureș, Romania, pp. 6–29.
14. VASILEVICH, Y.V. & DOUNAR, S.S. (2017) Finite element analysis of centreless-lunette turning of heavy shaft. *Science & Technique* 16(3), pp. 196–205.
15. VASILEVICH, Y.V., DOUNAR, S.S. & KARABANIUK, I.A. (2016) Finite element analysis of concrete filler influence on dynamic rigidity of heavy machine tool portal. *Science & Technique* 15(3), pp. 233–241.
16. VASILEVICH, Y.V., DOUNAR, S.S., TRUSKOVSKY, A.S. & SHUMSKY, I.I. (2015) Modeling and analysis of dynamics in bearing system of drilling, milling, and boring machine with mono-column. *Science & Technique* 3, pp. 9–19.
17. ZIENKIEWICZ, O.C. & TAYLOR, R.L. (2000) *The finite element method. Volume 1: The Basis*. Fifth edition. Oxford: Butterworth-Heinemann.

Cite as: Dounar, S. & Jakubowski, A. (2021) Dynamic finite element analysis of rotor-shaft fastening into a heavy precise lathe. *Scientific Journals of the Maritime University of Szczecin, Zeszyty Naukowe Akademii Morskiej w Szczecinie* 66 (138), 37–45.